Journal of Sound and Vibration (1999) **223**(5), 795–819
Article No. jsvi.1999.2157, available online at http://www.idealibrary.com on IDEAL®

SCALE MODELLING OF SOUND PROPAGATION IN A CITY STREET CANYON

K. V. Horoshenkov, D. C. Hothersall and S. E. Mercy*
Department of Civil and Environmental Engineering, University of Bradford, Bradford BD7 1DP, England

(*Received* 3 *July* 1998, *and in final form* 12 *January* 1999)

Acoustic scale modelling is used to study sound propagation in a city street canyon. The acoustic performance of several noise abatement schemes is investigated at various receiver heights for noise fields produced by different categories of vehicles travelling in the two lanes. The results are discussed in terms of the attenuation rate predicted along the canyon and the insertion loss. It is shown that although the effects produced by complex noise abatement schemes are significant they cannot be predicted by simple addition of the effects from the individual components of the schemes.

1. INTRODUCTION

In urban areas buildings are often constructed near busy roads and expressways. This proximity results in complex reflection and scattering effects leading to increased sound levels which may exceed the recommended limits. The confined space between the road and the facades poses problems in assessing the acoustic performance of many conventional noise abatement schemes. Alternative non-traditional noise abatement schemes can be expensive and complex to implement, therefore a special study is required to predict their acoustical performance and cost effectiveness.

The principal aim of these experiments has been to investigate the effect of a canyon street when noise is emitted by traffic in the vicinity of the impedance ground and repeatedly reflected from two parallel building facades. Although this problem has been addressed in the past, most of earlier studies [1–5] have mainly focused on the problem of predicting the attenuation of sound propagating from an individual vehicle along the street and contain limited information on the effects of multiple reflections on the performance of absorbing surfaces and road noise barriers.

A typical city street is therefore formed by two parallel sets of buildings with occasional gaps where side streets occur and, sometimes, by other structural complexities. The main effect considered in this work is of multiple reflections of

*Mechanical Sciences Sector, DERA, Farnborough, Hampshire, GU14 0LX, England.

0022–460X/99/250795 + 25 $30.00/0

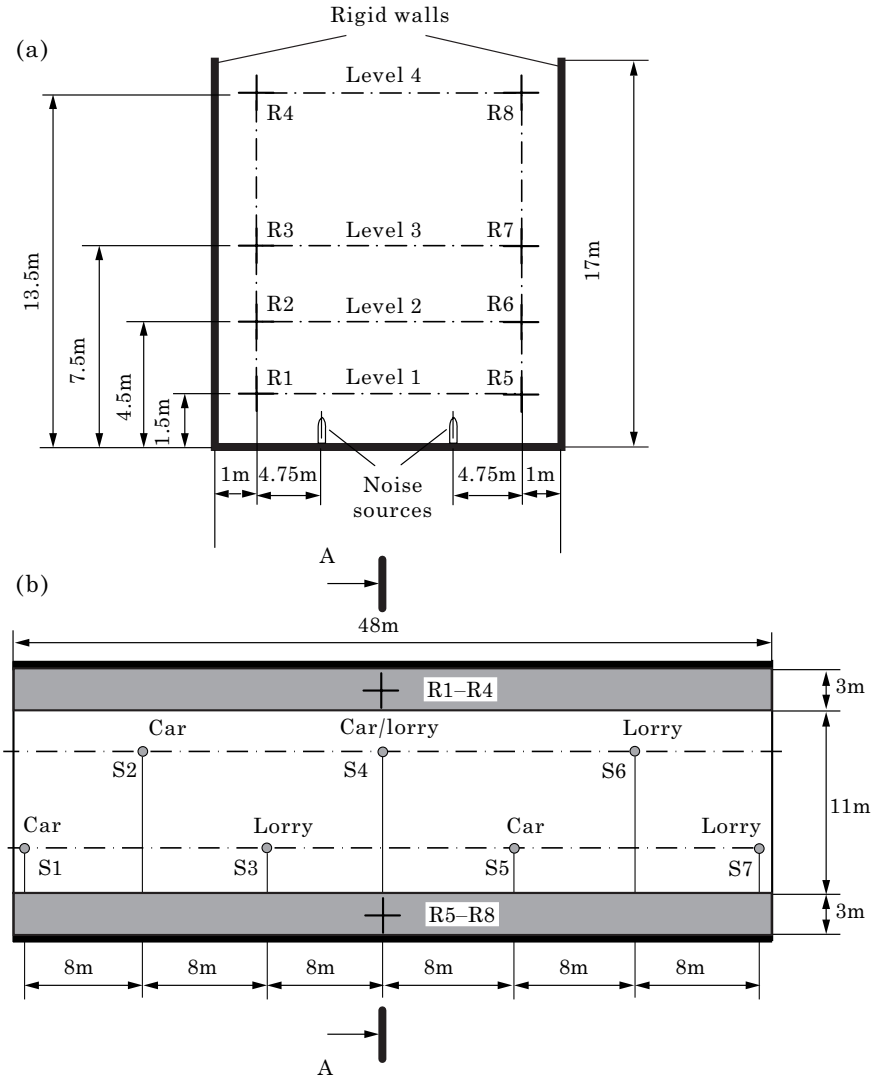

Figure 1. Full scale diagram of the experimental model: (a) Section A–A; (b) plan view.

traffic noise. These reflections occur at the building facades and the ground and can be a very substantial contribution to the overall sound levels. To model this effect a 1:20 scale model of such a street has been built in the anechoic chamber and used in this study.

Most of the typical problems related to the scale modelling technique have been resolved before the main course of the model experiments has commenced. Some attempts have been made to estimate the effects of air absorption on the results. Full allowance for this effect would require a considerable effort and cost and these resources were not available at the time.

This paper is organised in the following manner. Section 2 reports the development of the experimental model used to study the propagation of noise

in a typical city street in which the so-called "canyon effect" is set up. The methods used to overcome the difficulties related to the problem of scale modelling are discussed here in detail. A short discussion is given to the validity of the methods, equipment and materials used in the scale modelling. The actual experimental results on various abatement methods are presented in section 3 in which the efficiency of the individual methods and their combinations is analysed in terms of the insertion loss and the attenuation rate along the street canyon. Finally, recommendations are made and conclusions are drawn in section 4.

2. EXPERIMENTAL SCALE MODEL

2.1. PHYSICAL CONFIGURATION

In order to study the multiple scattering effect and the efficiency of different abatement techniques, a 1:20 model of a canyon has been set up in the anechoic chamber (Figure 1). In its basic layout, the model has a flat rigid floor and two parallel rigid walls sitting upon it. All the surfaces are made of 18 mm medium density fibreboard covered with a thin layer of Formica to ensure a good approximation to a rigid surface over the extended frequency range. At full scale the model represented a section of a 48 m long street with two 17 m high flat vertical parallel building walls erected on either side of the road (corresponding to approximately 5 storeys) and separated by 11 m of the road surface and two 3 m pedestrian footways. This is fairly close to the values used by several other authors [4, 5].

Eight receiver positions (R1–R8) have been defined at the central cross-section of the street, four on either side of the road at 1 m from the building facade to investigate the vertical distribution of the noise levels radiated by the vehicles travelling in the near and far side lanes.

Seven ultrasonic sources [6] S1–S7 have been distributed along the road to simulate noise from the traffic on two lanes (Figure 1). The sources have been supplied with air from pipes beneath the floor of the model. Light and heavy vehicles have been simulated by tubes from the source chambers elevated at $h_s = 0{\cdot}025$ m (0·5 m at 1:20 scale) and $h_s = 0{\cdot}05$ m (1·0 m at 1:20 scale) above the surface, respectively. The spectrum for every whistle (2–80 kHz) has been numerically adjusted (see Appendix A) during the postprocessing to comply with standard light and heavy vehicle spectra (100–4000 Hz) [7]. Several arrangements of absorbers and pedestrian restraints (low profile barriers) have been selected for the study and organised as individual experimental design "modes". These are listed in Table 1 and Figures 2(a–d).

The accuracy of acoustic scale modelling strongly depends on the choice of porous absorbing materials with properties at the scale frequencies which resemble those of full size absorbers. In this study the Attenborough impedance models have been used to identify a combination of microscopic parameters which ensures that the surface impedance is scaled correctly at the model frequencies. On this basis a representative selection of materials for scale

TABLE 1
Experimental modes

Mode No.	Code	Figure 2	Treatment	Absorber(s)
1	RG, Reference	(a)	none	none
2	AG	(a)	ground	8 mm *Coustone*
3	CAW	(a)	walls	wool felt HW25
4	AG + CAW	(a)	ground/walls	*Coustone*/wool felt
5	AF + CAW	(a)	footways/walls	*Coustone*/wool felt
6	IAW	(b)	walls	hear–jute felt
7	AG + IAW	(b)	ground/walls	*Coustone*/hair–jute felt
8	RPR	(c)	curb-sides	none
9	APR	(c)	curb-sides/facades of restraints	hair–jute felt
10	AG + APR	(c)	ground/curb-sides	*Coustone*/hair–jute felt
12	AG + CAW + APR	(d)	ground/walls/curb-sides	*Coustone*/wool felt
13	AG + IAW + APR	(d)	ground/walls/curb-sides	*Coustone*/hair–jute felt
14	IAW + RPR	(d)	walls/curb-sides	hair–jute felt
15	IAW + RPR + CRB	(d)	walls/curb-sides/road's midspan	hair–jute felt

In Table 1 the following coding system has been used in the experiments: RG rigid ground and rigid walls; AG absorbing ground (8mm of *Coustone*); AF absorbing pedestrian footways (150 × 2400 × 8 mm strips of *Coustone*); CAW continuous absorbers on the walls (150 mm wide strip of 6·5 mm of wool felt HW25); IAW intermittent absorbers on the walls (squares of 150 × 150 × 10 mm of hair–jute felt); RPR rigid pedestrian restraints (150 × 50 mm^2, 10 mm of aluminium); APR restraints with the absorbing front (150 × 50 mm^2, 10 mm of hair–jute felt); CRB absorbing central reservation barriers (150 × 50 mm^2, 10 mm of hair–jute felt).

modelling has been made. The selected materials have been tested and used in the experiments. The theory and methodology for the selection and the selection itself are discussed in greater detail elsewhere [8].

An 8 mm layer of epoxy bond fine flint aggregate material (marketed under the tradename Coustone) was used to simulate a full scale porous asphalt absorbing ground surface with typical agregate and binder composition and thickness 150 mm [8]. High quality wool felt, 6·5 mm in thickness was used to simulate full scale continuous absorbers of average performance.

The continuous absorbers (Figure 2(a)) extended along the full length of the street. An intermittent treatment of the walls in the form of hair–jute squares

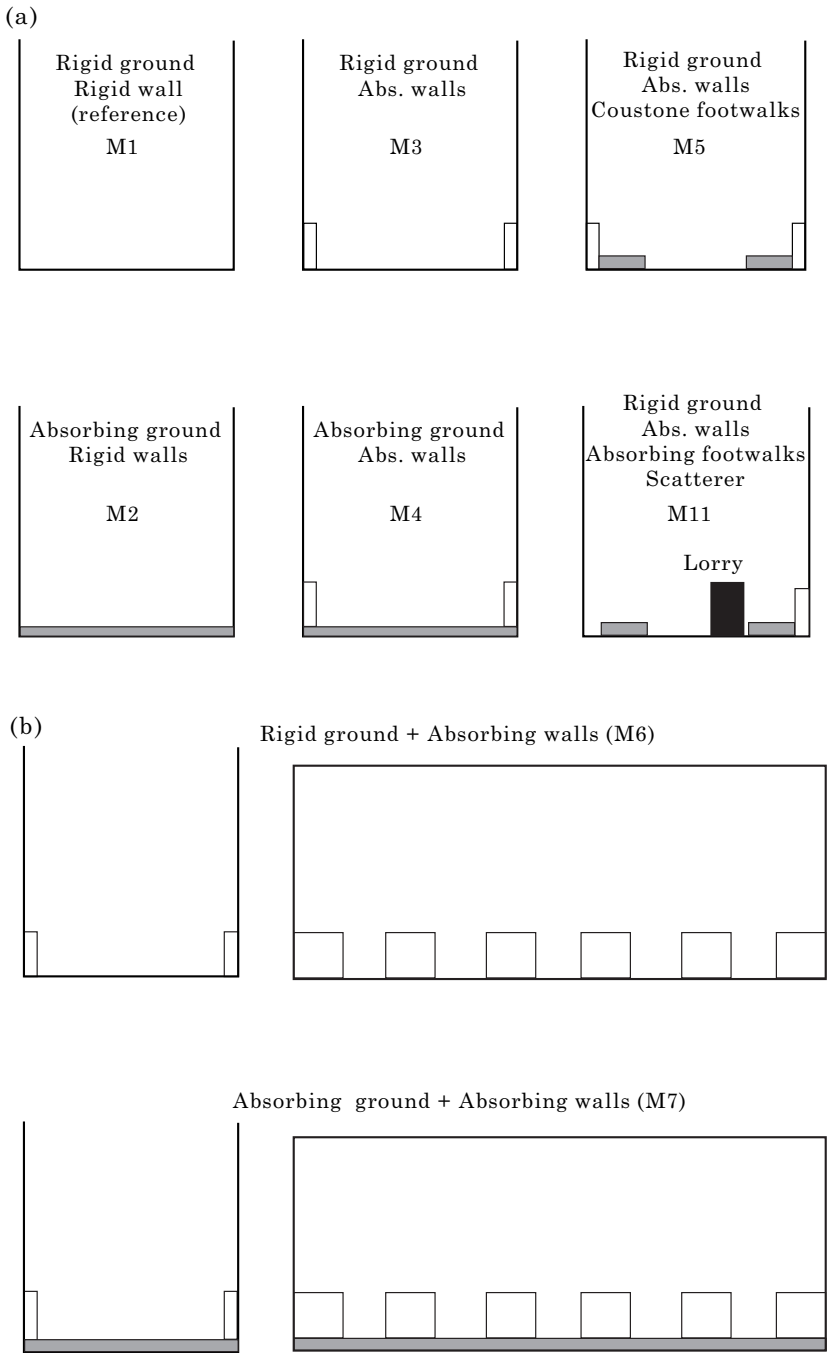

Figure 2. (a) Continuous absorbers (▨, 8/14 mm *Coustone* layer; □, wool felt; ■, rigid surface); (b) intermittent absorbers; (▨, 8 mm *Coustone* layer; □, hair–jute felt); (c) pedestrian restraints; (key as for 2(b) plus ■, rigid surface); (d) combined experiments; key as for 2(c).

(c)

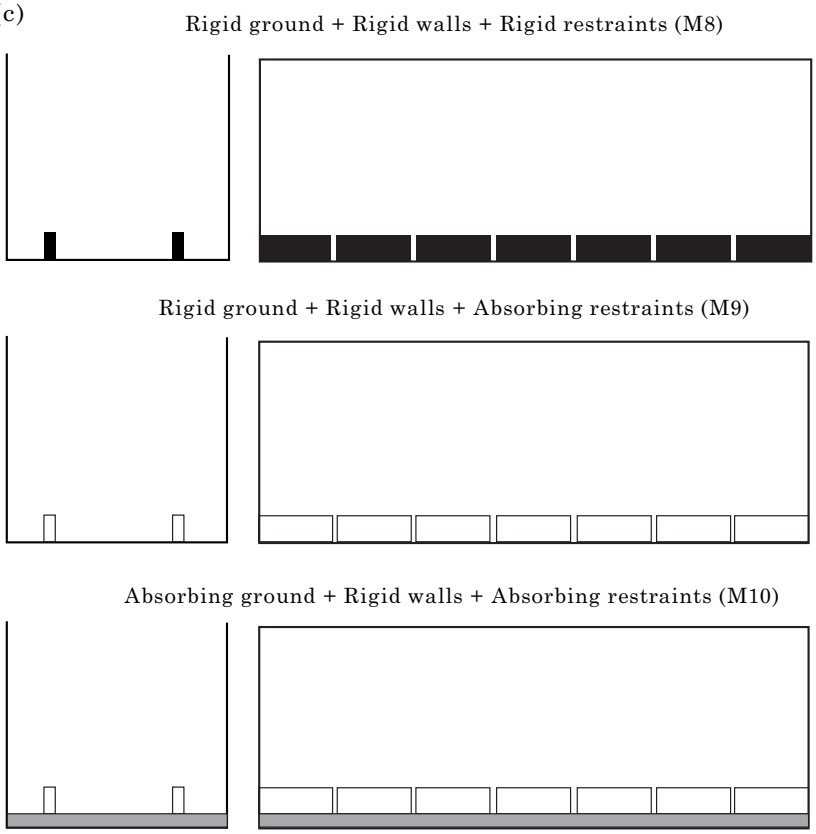

periodically arranged with a 150 mm interval (Figure 2(b)) has been considered more practical than a treatment with continuous absorbers which do not allow for features on the facades, e.g., windows, doors, signs, etc. The material of these squares was 10 mm hair–jute felt which had substantially higher values of the absorption coefficient than that of the continuous absorbers. This was a compromise between the area of the covered surfaces and the effectiveness of the absorber.

Pedestrian restraints have been arranged along the full length of the model street above the kerb lines and elevated at 10 mm above the surface. The individual restraints were separated from each other by 20 mm gaps (Figures 2(c) and (d)). The use of the discrete restraints instead of a continuous barrier has been considered to be a more practical design which allowed easy access between the road and the pedestrian areas. Absorbing treatment has been only allowed to the surface of the restraints facing the traffic and in this case the absorbers have been attached to 1 mm aluminium backing plates. The central reservation barrier had the same dimensions of the pedestrian restraints, but was treated with a 10 mm layer of hair–jute felt on both sides.

(d)

Absorbing ground + Absorbing walls + Absorbing restraints (M12)

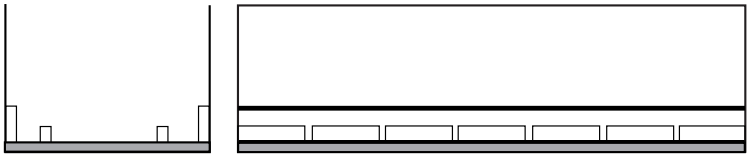

Absorbing ground + Absorbing walls + Absorbing restraints (M13)

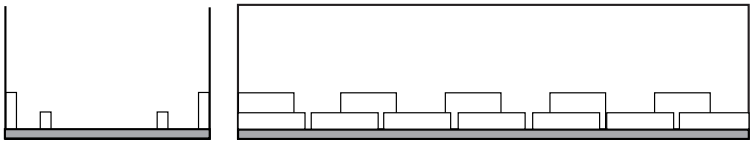

Rigid ground + Rigid walls + Absorbing restraints (M14)

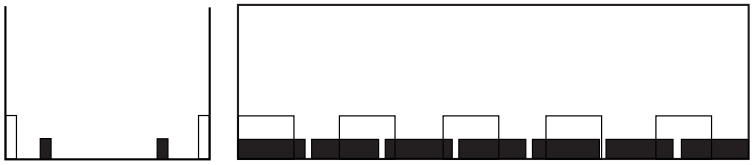

Rigid ground + Absorbing walls + Rigid restraints + Absorbing central reservation barrier (M15)

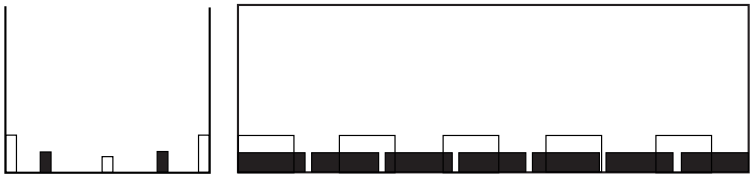

The change of sound levels from individual vehicles with distance along the street, the vertical distribution of sound levels from individual vehicles and the vertical distribution of sound levels from a steady traffic flow have been investigated. The levels obtained from every experiment have been compared to the data measured in the case of sound propagation over rigid ground between two parallel rigid walls. From this comparison the fundamental figures for the insertion losses have been deduced. The latter indicated the quality of the abatement scheme tested.

2.2. ADJUSTMENT OF THE ULTRASONIC NOISE SPECTRUM

The noise spectrum emitted by the model source does not reproduce the standard spectra of light and heavy vehicles [7], but may be numerically adjusted

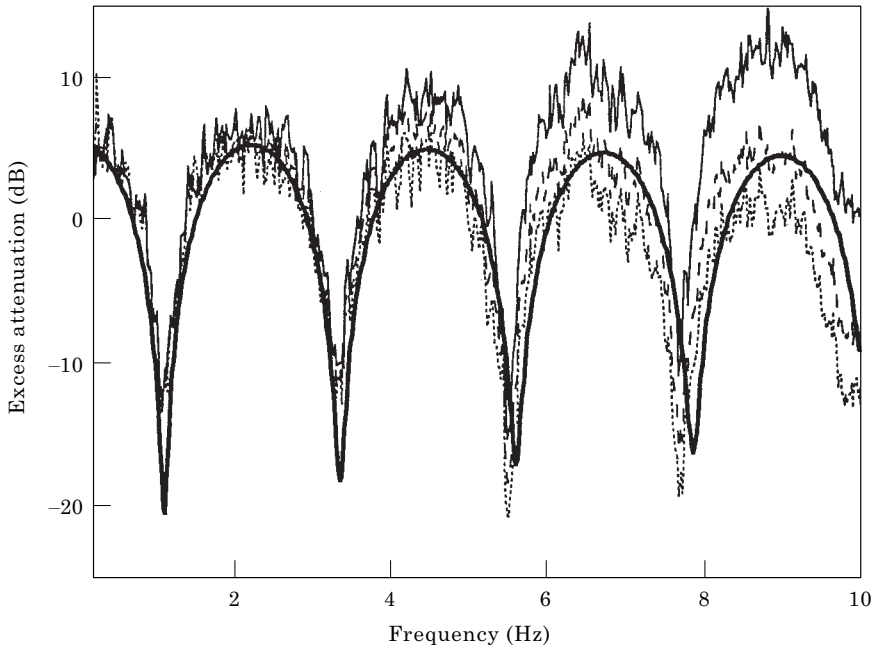

Figure 3. Influence of the microphone orientation on the excess attenuation for sound propagation above the rigid ground. The source is at 0·025 m above the rigid ground. The receiver is 0·237 m from the source and suspended at 0·075 m above the ground. Key: —, theory; experimental reference: —, normal; – – –, averaged; · · · · · ·, direct.

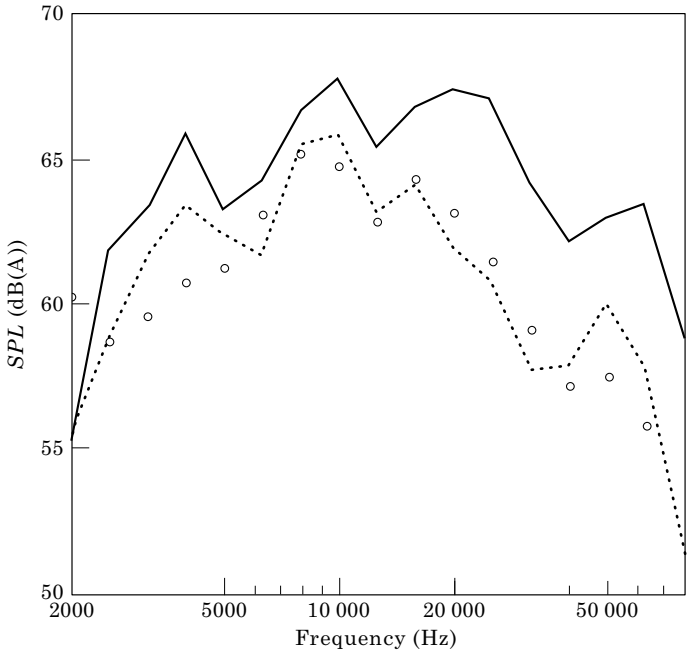

Figure 4. Effect of the air absorption on the corrected spectrum emitted by the model source S7 (0·05 m). The microphone is suspended at the receiver position R1 above the rigid ground (see Figure 1). Key: —, theory no absorption; – – – –, theory RH 45% T = 20°C; ○, experiment RH = 45% T = 20°C.

for each individual whistle and A-weighted before the broad band *SPL*'s are calculated. A formal description of this approach is given in Appendix A.

In the following discussion one is mainly interested in the excess attenuation defined as

$$EA = L_A - L_A^{(f)} \tag{1}$$

and the insertion loss

$$IL = L_A^{(0)} - L_A. \tag{2}$$

Here L_A is the A-weighted *SPL* measured in the street for a given noise abatement scheme, $L_A^{(f)}$ is the A-weighted *SPL* measured in free field and $L_A^{(0)}$ is the *SPL* in the street when all the surfaces are rigid.

2.3. MICROPHONE

The receiver is, probably the most important element in conducting accurate model tests of complex acoustic environments. In this case errors are related to the lack of omni-directionality and frequency dependent sensitivity of the microphone as the frequency of the sound increases. The problem is relatively easy to compensate for if the path of the incident sound is clearly defined so that the directivity of the receiver can be included in the computations. This compensation is not possible in the case when sounds emitted by multiple sources are reflected many times in the model before they are received.

Measurements have been carried out to obtain the reference data to adjust the model spectra and to include the effects of the directivity in the Brüel & Kjær type 4138 1/8 in microphone employed in the experiments. In the absence of the walls two tests have been performed on each individual source used in the scale model experiments. In the first test the microphone has been placed on the ground and oriented so that the source lay in the plane of the diaphragm (normal position for a pressure response microphone). In the second test the microphone position has been changed so that the normal to the plane of the diaphragm passed through the source (direct position). The mean spectrum for the model source in equation (19) is assumed to be given by

$$\hat{p}_v(\omega) = (1/2\kappa)(\hat{p}_v^{(dir)}(\omega) + \hat{p}_v^{(norm)}(\omega)), \tag{3}$$

where $p_v^{(dir)}$ is the sound pressure spectrum measured in the direct position and $p_v^{(norm)}$ is the sound pressure spectrum measured in the normal position at the same distance from the source. The effect of the ground is accounted for by dividing the mean spectrum by the factor $\kappa = 2$. Figure 3 demonstrates the effect of the microphone orientation on the excess attenuation spectrum which is adjusted using relations (21) and (22). The spectrum is compared to that predicted by the image source model [9] for an omni-directional receiver. The graph suggests that the mean spectrum of the reference signal is the most appropriate to account for directionality of the microphone and this has been used in all further computations of the experimental spectra. Here the reference signal $\hat{p}_{ref}(\omega)$ is obtained when the microphone is laid on the ground and its

orientation is altered. At any other position (R1–R8) within the experimental model the microphone is suspended by its cable and directed strictly towards the ground.

Another important factor in producing random errors is the accuracy of positioning of the microphone. The most typical result of mispositioning is a shift of the interference pattern in the pressure spectrum. Care has been taken to ensure the accuracy in positioning to ± 1 mm ($\sim 1/4$ wavelength at 80 kHz).

2.4. THE AIR ABSORPTION

To investigate the effect of air absorption the results from the experimental model have been compared with the predicted using a three-dimensional image source model. In this model the ANSI S1.26-1978 standard procedure for computing the values of the air absorption in gases has been adopted [10]. The absorption has been included in the model as the complex part of the wavenumber $k' = k + \mathrm{i}\alpha$, where α is calculated according to the standard and has dimension of metre^{-1}.

This modification has been tested by conducting an experiment in the presence of walls above the acoustically rigid ground. The most remote source S7 has been selected for this test and the microphone has been set up in position R1 (see Figure 1). The temperature and the relative humidity have been monitored and recorded in the course of the experiments so that the absorption could be accurately calculated. The comparison between the experimentally measured 1/3 octave *SPL*'s with those predicted from the image source model using spherical wave Green's function for 80 images for $\alpha = 0$ and for finite values of the absorption is shown in Figure 4. It can be seen from the graph that the maximum discrepancy between the theory and the experiment occurs at the upper end of the spectrum and can reach up to 5–6 dB. These figures are substantial for the direct comparison between the model *SPL* spectrum and the spectrum predicted, for example, from a full scale test. Nevertheless, it is suggested that there is likely to be some compensation if the *insertion losses* are deduced from scale model tests performed in similar atmospheric conditions. Also, in a real city street the building facades will have a reflection coefficient $V < 1$ so that sound energy would be irretrievably lost on every reflection. This may produce an analogous effect to that of air absorption which will be neglected in the following discussion.

2.5. BOUNDARY LAYER EFFECT

Another potential source of error in scale model experiments is from the boundary layer effect which results in an apparent non-zero admittance of the rigid boundary to an incoming plane wave. The influence of the boundary layer on the sound field reflected by a rigid plane in scale modelling experiments has been discussed by Almgren [11]. The expression for the normalised surface admittance presented is given by [11]

$$\beta_s = (1/\sqrt{2})(1 - \mathrm{i})(\omega\mu/\rho_0 c^2)^{1/2}(\sin^2\theta_0 + (\gamma - 1)N_{pr}^{-1/2}). \tag{4}$$

This can be used to estimate the value of the effective flow resistivity in the two-

parameter Attenborough model [12]. In (4) θ_0 is the angle of incidence, μ is the dynamic viscosity of air, N_{pr} is the Prandtl number, γ is the ratio of specific heats and the other parameters are given in the list of notation.

Assuming that $f/R_e < 1$ and equating expressions [12]

$$\beta_s = (\gamma\rho_0\pi)^{1/2}(f/R_e)^{1/2}(1-i) = 2{\cdot}30(f/R_e)^{1/2}(1-\mathrm{i}), \tag{5}$$

and (4) one obtains for the effective flow resistivity

$$R_e = \rho_0 c(\gamma/\mu)^{1/2}(\sin^2\theta_0 + (\gamma-1)N_{pr}^{-1/2})^{-1}. \tag{6}$$

If the angle of incidence $\theta_0 \cong \pi/2$, then the effective flow resistivity required to account for the boundary layer effect is of order 10^{10} N s m^{-4}. This value will increase for angles of incidence $\theta_0 < \pi/2$.

2.6. ANALOG–DIGITAL CONVERSION AND FFT PROCESSING

Computer software has been developed to implement the fast Fourier transform algorithm and the 1/3-octave filter analysis. The program has been checked for some definitive signals against spectral estimations obtained from a Brüel & Kjr 2033 FFT analyser within its operational frequency range. The results for the comparison have agreed extremely well.

The signal/noise ratio within the actual electronic channel has been better than 60 dB. A Hanning window has been used in the signal processing algorithm. The distortion of the spectrum has been estimated as less than 0·1% because 32 time data sets have been used to generate the average spectrum [13].

2.7. REPEATABILITY AND REPRODUCIBILITY

Repeatability and reproducibility tests have also been conducted to quantify the extent of the random errors in the final results. The repeatability of the experiments has been tested with the street layout corresponding to the mode 11 (see Figure 2(a)). The data acquisition has been triggered twice for the same microphone position (R8) and for the same ultrasonic whistle (S5), but with a twenty four hour interval. No alteration has been introduced to the model itself and all the instrumental settings in the second test have been identical to those in the first test. The difference in the measured 1/3 octave *SPL*'s is between ± 1 dB(A) for frequencies above 2000 Hz at which a 2 dB signal-to-noise ratio has been maintained in the experiments. This produced an error in the broad band level within 0·1 dB(A).

A reproducibility test has been also carried out by a second investigator. The walls in the model have been removed, then erected and adjusted again. Experiments have been repeated for the mode 1 (see Figure 2(a)). The broad band *SPL*'s emitted by various sources have been compared to those obtained in the original experiment in Table 2. The experimental conditions (air pressure, microphone, amplifications, length of the realisations, number of the realisations) have been the same for the two sets of results.

The maximum discrepancy between the results from these broad band *SPL* is 0·6 dB(A) and it is felt that the reproducibility is adequate. On the basis of this

TABLE 2
Discrepancy in the broad band SPL levels

Mode	Source	Receiver position	Level difference, dB(A)
1	1	R1	0·60
1	3	R1	0·25
1	5	R1	0·04
1	7	R1	0·26

comparison the decision has been made to confine the number of samples for each signal realisation to 1024 while the actual number of the realisations in each independent experiment ("source-receiver") has been kept at 32.

2.8. COMPARISON WITH OTHER PUBLISHED RESULTS

Results for excess attenuation for sound propagation between two parallel rigid walls and above rigid and absorbing ground have been compared with other published results [4, 5] for the reduction in sound pressure level as the vehicle travels away from the receiver plane (Section A–A in Figure 1). These are graphically illustrated in Figure 5. The comparison is only valid for for the

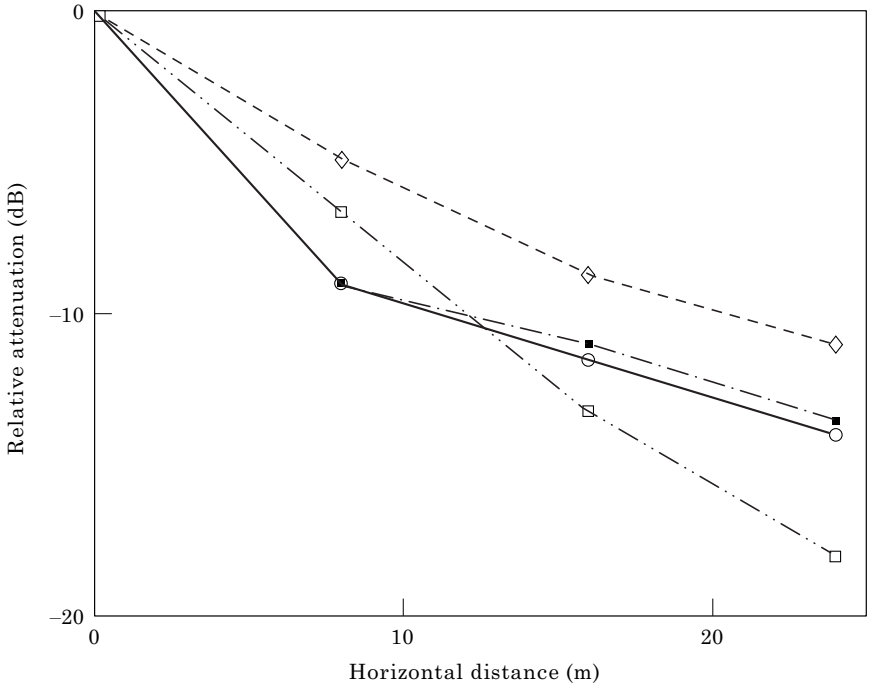

Figure 5. Comparison of the relative attenuation for noise generated by two light vehicles travelling simultaneously in the opposite lanes of the canyon. Key: —○—, scale model; –·■–·, ISM; –··□··–, Hewtschi; ––◇––, Radway and Oldham.

configuration with rigid ground and wall surfaces, but results for staggered facades are also available [4]. Similar trends are observed from the comparison.

3. EXPERIMENTAL RESULTS

3.1. DOWNSTREET ATTENUATION

The information about the attenuation of sound propagating along a street from an individual vehicle has two potential applications. The first application is related to the values of the equivalent continuous noise level, L_{eq}, measured under interrupted flow conditions. The equivalent continuous noise level is largely influenced by the sound energy which propagates from distant traffic if the attenuation of sound along the street is small. This is likely to result in higher values of L_{eq} compared to the case when the level is measured for the same traffic conditions, but in the absence of the walls.

The second application is related to the problem of noise emitted into streets adjacent to the main road. In this situation, the measured levels of L_{eq} will depend upon the attenuation rate down the side street and can be relatively easily predicted if this effect is quantified.

In order to characterise the attenuation by a single coefficient we assume that sound energy decays according to the power law y^{-b}, where y is the distance measured between the receiver plane and the vehicle(s). So that the expression for the sound pressure level is written as

$$SPL = 10\log_{10}(\langle p^2(y)\rangle/p_0^2) = 10\log_{10}\{\langle p_{ref}^2\rangle/p_0^2 y^{-b}\}$$
$$= 10\log_{10}\langle p_{ref}^2\rangle/p_0^2 - 10b\log_{10} y, \tag{7}$$

where $\langle p_{ref}\rangle$ is the free field reference pressure which is measured at 1 m from the source and $p_0 = 2 \times 10^{-5}$ N/m^2.

The coefficient b can be evaluated by the least mean squares method [13] if N SPL's measured along the street are known for N values of y. In this method one has to minimise the difference

$$D = \sum_{i=1}^{N-1}(\Delta SPL_i - 10b\log_{10} y_i)^2, \tag{8}$$

where

$$\Delta SPL_i = SPL_i - SPL_{ref}, \quad SPL_i = 10\log_{10}(\langle p^2(y_i)\rangle/p_0^2) \tag{9}$$

and

$$SPL_{ref} = 10\log_{10}\langle p_{ref}^2\rangle/p_0^2. \tag{10}$$

Figures 6(a) and (b) show the effect of rigid (Mode 1) and absorbing (Mode 2) ground on the sound levels produced by the two types of vehicle in the near- and farside lanes. The absorbing surface results in the decreased values of SPL

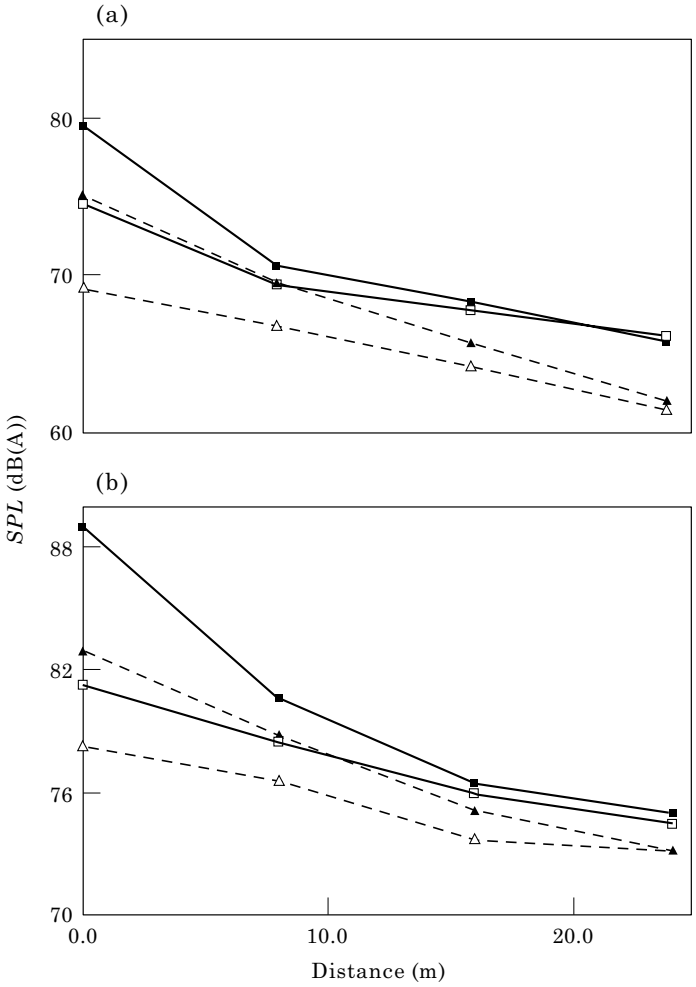

Figure 6. Effects of the absorbing ground on the sound pressure levels generated by a light (a) and by a heavy (b) vehicle in the nearside and the farside lanes. Key: —■—, RG(*n*); —□—, RG(*f*); – –▲– –, AG(*n*); – –△– –, AG(*f*).

throughout the range of y. The levels from nearside and farside vehicles passing the receiver plane differ by about 4–6 dB(A) and their behaviour is asymptotically similar as the distance y increases. For the light vehicles the effect of the absorbing surface results in a more uniform slope of the graph (Figure 6(a)) throughout the range of y compared to the case of rigid ground.

A second way of assessing the variation of *SPL* with distance along the street is to combine the data for near- and farside vehicles at the same cross-section of road. This can be expected to provide a more stable trend. The attenuation parameter b as defined in equation (8) was determined for each case and is given in Table 3.

The combined results for the *SPL* at pedestrian height from near- and farside vehicles at the same cross-section on the road are plotted in Figures 7–10 for

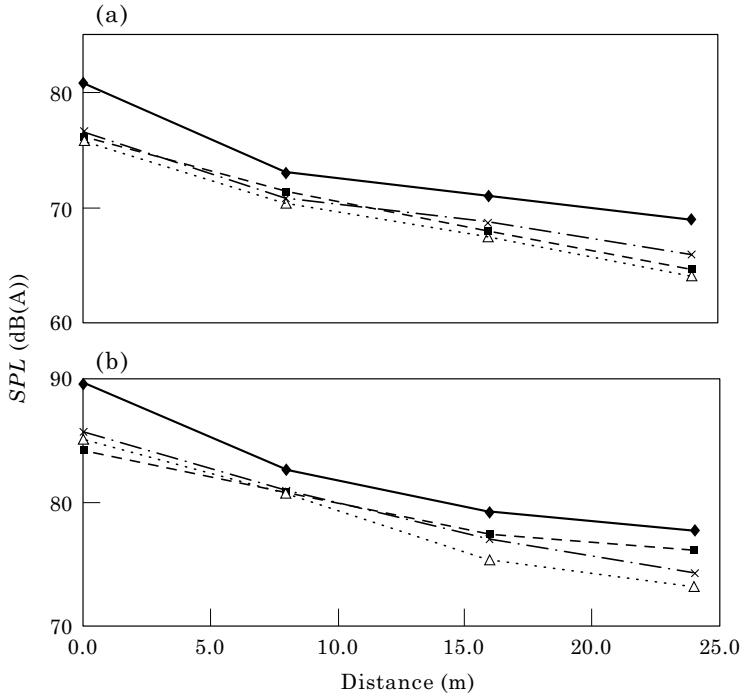

Figure 7. Sound pressure levels emitted by light (a) and heavy (b) vehicles in the near- and far-side lanes at the same cross-section in the presence of absorbing ground (AG); continuous absorbers on the walls (CAW); intermittent absorbers on the walls (IAW). Key: —◆—, RG; – –□– –, AG; · · · △ · · ·, CAW; · – × · –, IAW.

light and heavy vehicles as a function of distance along the street. The effects of the absorbing road surface, absorbing walls, pedestrian restraints and their combinations can be seen.

Figures 7(a) and (b) show the effect of the absorbing ground, and also continuous and intermittent absorbers on the walls. In the case of the light vehicles the effectiveness of the proposed treatments is comparable for different values of y. In the case of the heavy vehicles the performance of the walls' treatment becomes superior to that of the absorbing ground as y increases.

Figures 8(a) and (b) show the effect of the pedestrian restraints with a rigid and an absorbing face. It can be seen from the graphs that the difference in the performance between these two types of restraints is only noticeable for the light vehicles and greater values of y. The largest effect is achieved when the vehicles are close to the receiver plane.

The most pronounced effect of combinations of absorbing surfaces in Figures 9 and 10 is not merely the absolute reduction in the *SPL*, but the faster attenuation rate resulting in greater values of the coefficient b (see Table 3). In every scheme which involves the use of pedestrian restraints in the presence of rigid ground one can identify a substantial reduction in noise levels only if the vehicles are close to the receiver plane, while the absorbing ground in combination with these and other simple schemes positively affects the attenuation rate.

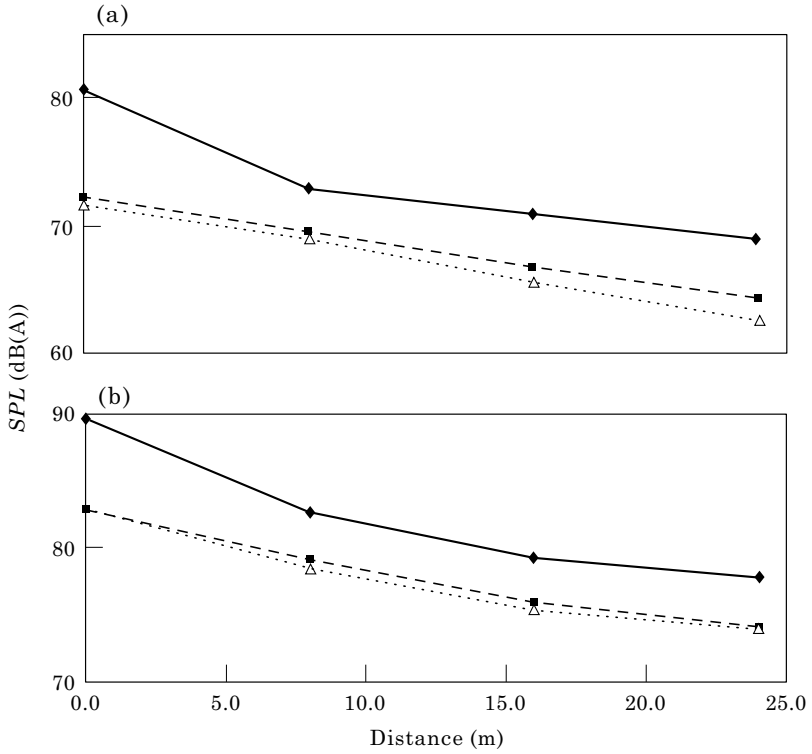

Figure 8. Sound pressure levels emitted by light (a) and heavy (b) vehicles in the near- and far-side lanes at the same cross-section in the presence of rigid restraints (RPR) and absorbing pedestrian restraints (APR). Key: —·—, RG; – –□– –, RPR; · · · △ · · ·, APR.

Table 3 shows the values of the coefficient b deduced from the results presented in Figures 7–10. It can be seen from this table that even for the same mode the rate at which sound attenuates largely depends upon the height of the source (light or heavy vehicle). In mode 1 this rate is close to that attributed to cylindrical spreading for noise for the heavy vehicles and is less for the light vehicles.

The absorbing ground alone enhances the attenuation only if the source is relatively low while continuous absorbers on the wall show better effect for the higher position of the source. According to the results, the downstreet attenuation at this receiver height is enhanced from 2.6 dB (mode 1) to 4·1 dB per doubling in the distance, but only in the case of the light vehicles (low source height). The same scheme has the opposite effect when the noise is emitted by a heavy vehicle, although the change in attenuation is insignificant (3·2 dB compared to 3·0 dB per doubling of distance).

Continuous absorbers on the walls have a different influence on the downstreet attenuation to the intermittent. In this experiment the attenuation rate per doubling of distance increases to 3·9 dB and 4·9 dB in the case of a light

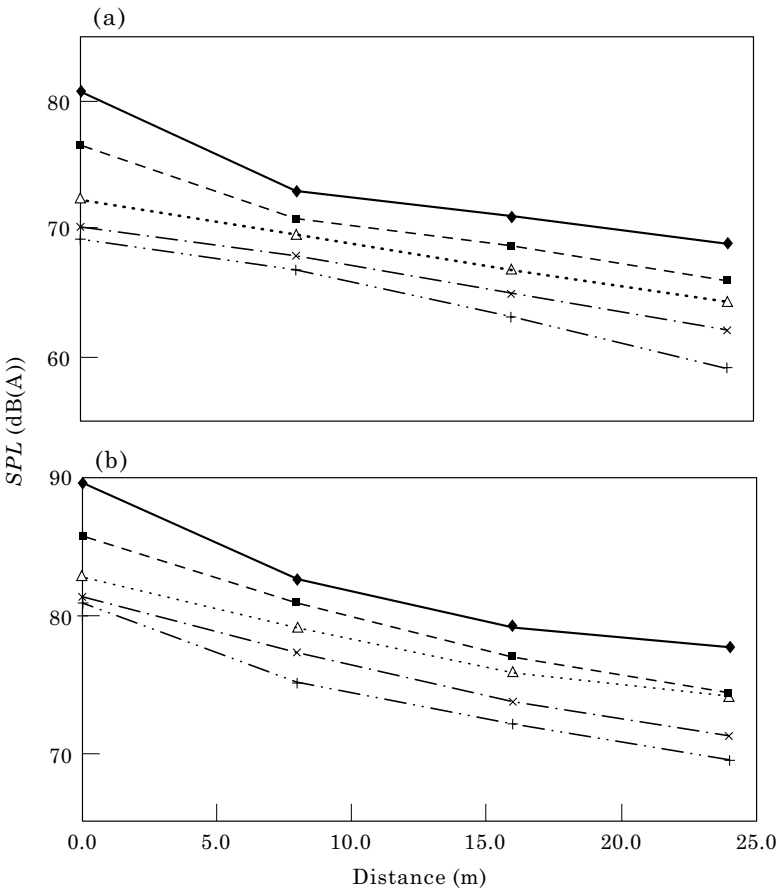

Figure 9. Comparison of the effects of several noise abatement schemes, including central reservation barrier (CRB), in the presence of rigid ground. Sound pressure levels are emitted by light (a) and heavy (b) vehicles in the near- and farside lanes at the same cross-section. Key: —◆—, RG; – –□– –, IAW; · · · △ · · ·, RPR; · –×– ·, RPR + IAW; ·· – + – · RPR + CRB + IAW.

and a heavy vehicle, respectively. The same effect is less pronounced if the absorbers are intermittent (3·0 dB and 4·1 dB, respectively).

Pedestrian restraints do not change significantly the attenuation rate for noise from either the light or the heavy vehicles from that experienced for the rigid conditions. The absorbing face on the pedestrian restraints results in a noticeable increase of the attenuation only for the low source height. In this case the attenuation rate is predicted as 4·0 dB per doubling of distance.

Apparently, the attenuation rate can be enhanced by these combinations of abatement schemes. This enhancement is substantial mainly for the light vehicles and is generally proportional to the amount of absorber introduced into the street. It is difficult to derive any consistent trend which would indicate how the combinations of the simple schemes affects the attenuation rate for noise emitted by light and heavy vehicles.

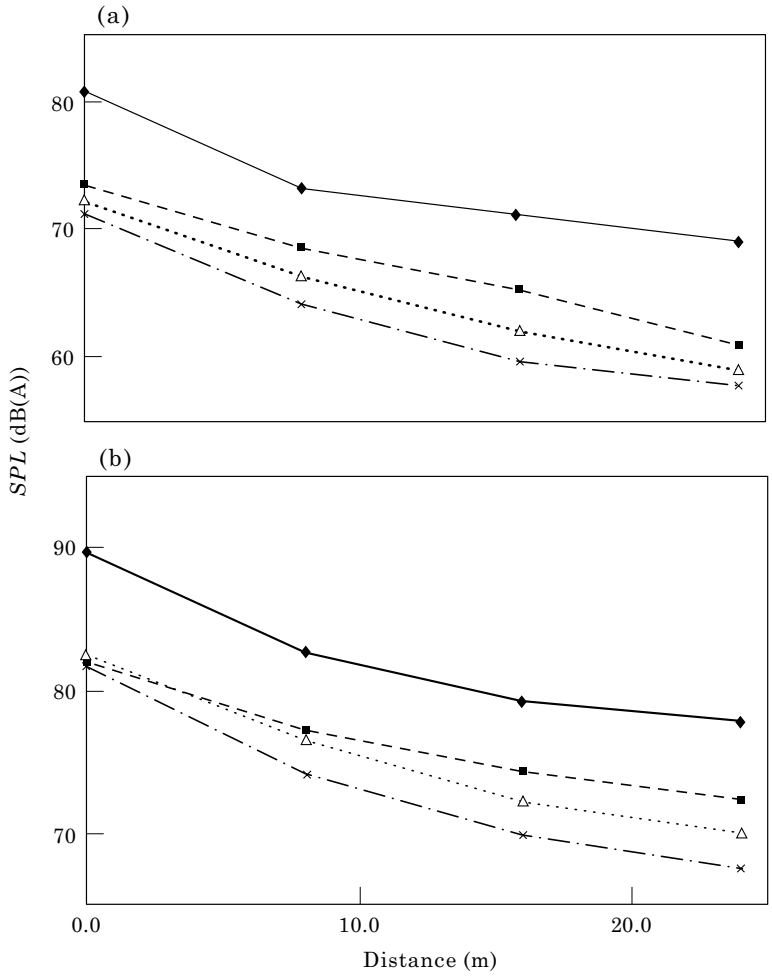

Figure 10. Comparison of the effects of several noise abatement schemes in the presence of absorbing ground. Sound pressure levels are emitted by light (a) and heavy (b) vehicles in the near- and farside lanes at the same cross-section. Key: —◆—, RG; – –□– –, AG + IAW; · · ·△· · ·, AG + APR; – · ×– · , AG + IAW + APR.

3.2. INSERTION LOSS

In this section the average insertion loss will be discussed, defined as

$$IL = SPL_r - SPL_t, \tag{11}$$

where SPL_r is the sound pressure level at a given receiver position resulting from two simulated traffic streams on the roadway in the absence of any noise abatement schemes and SPL_t is the sound pressure level at the same receiver position with a given noise abatement treatment. In this scenario the individual vehicle results have been combined to represent the noise field produced by 14 vehicles equidistantly distributed along the street.

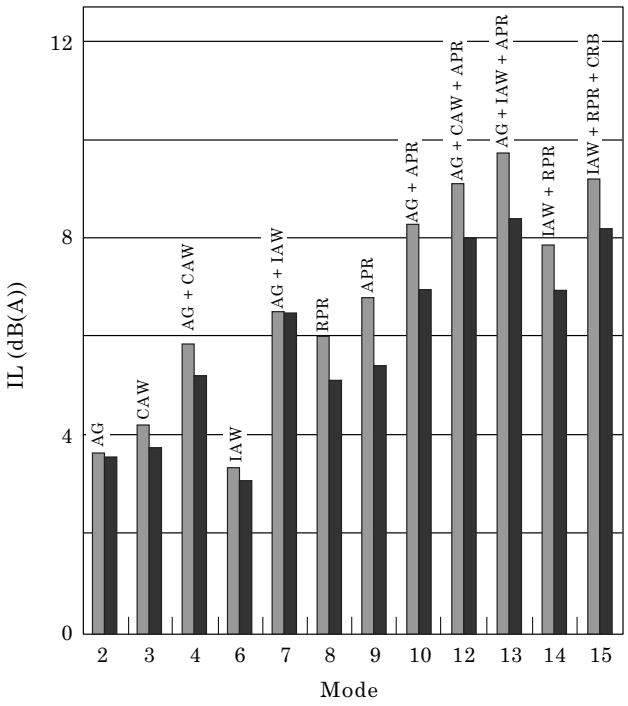

Figure 11. Insertion loss at the pedestrian height of 1·5 m. Key: ▨, light vehicles; ■, heavy vehicles.

Figure 11 shows the insertion loss at pedestrian height obtained for the twelve experimental modes. It can be seen from the figure that the schemes cause the maximum effect if the traffic is composed entirely of light vehicles, although the difference in the insertion loss between this case and the case of heavy vehicles is not substantial for the majority of modes.

It is convenient to list the proposed schemes according to their effectiveness at pedestrian height in terms of the computed average insertion loss (equation (11)). The results for the light and heavy vehicles are separated and can be used later in predictions of the insertion loss for noise from traffic with an arbitrary percentage of heavy vehicles.

In Figure 11 a consistent trend can be observed in the effectiveness of the noise abatement schemes for each category of vehicle. It is also possible to conclude that the maximum effect is observed when greater quantities of absorptive materials (or characteristic absorption $A = \sum S_i \alpha_i$, where S_i is the area treated with material having the absorption coefficient α_i) are introduced. Alternative schemes when rigid screens are used in combination with an absorbing central reservation barrier can also marginally reduce the levels of noise at the pedestrian heights. The presence of an absorber on the face of pedestrian restraints does not appear to be critical if the restraints are used independently from any other noise abatement scheme. Individual treatments

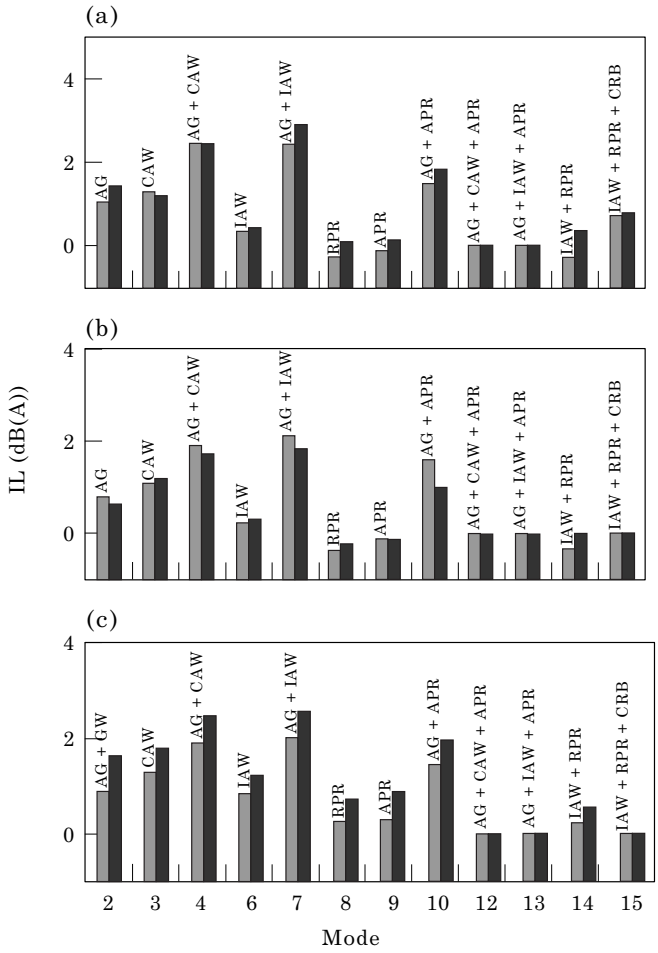

Figure 12. Insertion loss for greater receiver heights: (a) 4·5 m; (b) 7·5 m and (c) 13·5 m. Key as for Figure 11.

such as absorbing ground or absorbers on the walls produce reduction of 3–5 dB(A). The effect of combined treatments may not be described by addition of the results for the individual treatments either in terms of acoustic pressure or in terms of the reduction in acoustic energy.

The insertion loss observed for the absorbing ground is close to the maximum possible value of 3 dB(A) for non-coherent sources.

Considering the values of the insertion loss obtained at greater receiver heights (see Figures 12(a–c)), it is clear that the effectiveness of the proposed noise abatement schemes is greatly reduced and that the effects vary as the height changes. This can be explained by the fact that the acoustic treatment is confined to the vicinity of the ground and does not extend beyond the height of 3 m (absorbers on the walls). For this reason the following discussion will mainly focus on the effects observed at a height important for pedestrians and it will be assumed that the levels of sound at greater heights can be reduced by other

TABLE 3
Values of b for some noise abatement schemes

Mode No.	Code	Light vehicles	Heavy vehicles
Simple noise abatement schemes			
1	RG	0·85	1·05
2	AG	1·36	0·99
3	CAW	1·28	1·6
6	IAW	0·98	1·37
8	RPR	1·09	1·05
9	APR	1·35	0·97
Complex noise abatement schemes			
4	AG + CAW	1·88	1·33
7	AG + IAW	1·54	1·03
10	AG + APR	1·53	1·39
12	AG + CAW + APR	1·70	1·6
13	AG + IAW + APR	1·35	1·39
14	IAW + RPR	1·20	1·27
15	IAW + RPR + CRB	1·56	1·16

means, for example by those suggested in reference [14]. The use of pedestrian restraints can even cause negative values of insertion loss as a result of scattering of sound from the upper edge of the barrier towards the receiver position. This may provide an explanation to the fact that the effect of the majority of the proposed schemes has been negligible if the restraints have been included in the experiment. The maximum values of the insertion loss, of order 2–3 dB(A), have been achieved through the combination of the absorbing treatment of the road surface and the surface of the walls (modes 4 and 7) which resulted in the reduced contribution from the ground reflections to the overall level noise.

4. CONCLUSIONS

In this paper various aspects of the experimental scale modelling of sound propagation in a city street canyon have been discussed. For this purpose a new model facility has been developed. The acoustic performance of several noise

abatement schemes has been investigated at various receiver heights for noise produced by different categories of vehicles. Monopole sound sources have been used to represent the vehicles. The vehicle bodies were not simulated in the experiments reported here. It is possible that the scattering of sound from vehicle bodies would modify the results. Modelling of a few cases which included simple models of vehicles showed that they had an insignificant effect on the results. This is due to the average effect incorporated in the experimental method.

Two criteria of efficiency have been used in this investigation: attenuation rate along the street canyon and the insertion loss relative to the case when all the surfaces are rigid. The maximum reduction in the *SPL*'s has been achieved at pedestrian height for the combination of the following simple noise abatement schemes: absorbing ground, intermittent absorbers on the walls and absorbing pedestrian restraints (9·7 dB(A) for the light vehicles and 8·4 dB(A) for the heavy vehicles). The maximum attenuation rate for sound emitted by a light vehicle has been observed for a combination of absorbing ground and continuous absorbers on the walls. The maximum attenuation rate for sound emitted by a heavy vehicle has been observed for a combination of absorbing ground, continuous absorbers on the walls and absorbing pedestrian restraints.

Substantial effects have been observed only at the pedestrian height and the performance of the schemes at other receiver heights has been limited. Small negative values of the insertion loss have been obtained at these receiver heights if pedestrian restraints have been used independently from any other proposed schemes incorporating absorbing treatment.

The effect of combinations of the basic noise abatement schemes is complex and cannot be predicted by simple addition of the individual effects. The effects of these combinations are not additive either in terms of the acoustic energies or in terms of the acoustic pressures.

REFERENCES

1. R. Bullen and F. Fricke 1976 *Journal of Sound and Vibration* **46**, 33–42. Sound propagation in a street.
2. P. Steenackers, H. Myncke and A. Cops 1978 *Acustica* **40**, 115–119. Reverberation in town streets.
3. H. Kuttruff 1982 *Journal of Sound and Vibration* **85**, 115–128. A mathematical model for noise propagation between buildings.
4. D. J. Oldham and M. M. Radwan 1994 *Journal of Building Acoustics* **1**, 65–88. Sound propagation in city streets.
5. K. Heutschi 1995 *Journal of Applied Acoustics* **44**, 259–274. A simple method to evaluate the increase of traffic noise emission level due to buildings.
6. K. V. Horoshenkov and D. C. Hothersall 1993 *Proceedings of the Institute of Acoustics* **15**, 221–230. On the design of a broad frequency band source for scale modelling of sound propagation.
7. R. R. K. Jones 1979 *PhD Thesis*, *University of Bradford*. An investigation of road traffic noise characteristics in restricted flow situations.
8. K. V. Horoshenkov, D. C. Hothersall and K. Attenborough 1996 *Journal of Sound and Vibration* **194**, 685–708. Porous materials for scale model experiments in outdoor sound propagation.

9. K. V. HOROSHENKOV 1996 *PhD Thesis*, *University of Bradford*. Control of traffic noise in city streets.
10. *American National Standard* S1.26-1978 *Acoustical Society of America*. Method for the calculation of the absorption of sound by the atmosphere.
11. M. ALMGREN 1986 *Journal of Sound and Vibration* **105**, 321–337. Acoustic boundary layer influence on the scale model simulation of sound propagation: Theory and numerical results.
12. K. ATTENBOROUGH 1985 *Journal of Sound and Vibration* **99**, 521–544. Acoustical impedance models for outdoor ground surfaces.
13. J. S. BENDAT and A. G. PIERSOL 1988 *Random Data*. Wiley-Interscience.
14. D. C. HOTHERSALL, K. V. HOROSHENKOV and S. E. MERCY 1996 *Journal of Sound and Vibration* **198**, 507–515. Numerical modelling of the sound field near a tall building with balconies near a road.

APPENDIX A: ADJUSTMENT OF MODEL SOURCE SPECTRUM

If $\hat{p}_m(\omega)$ and $\hat{p}_v(\omega)$ are the broad band pressure spectra of the model source and the vehicle source then the A-weighted *SPL*'s of the model and vehicle sources can be written as

$$L_A^{(m)} = 10\log_{10}\left[\frac{4\pi^2}{p_0^2}\int_0^\infty |A(\omega)\hat{p}_m(n\omega)|^2\,\mathrm{d}\omega\right] \tag{12}$$

and

$$L_A^{(v)} = 10\log_{10}\left[\frac{4\pi^2}{p_0^2}\int_0^\infty |A(\omega)\hat{p}_v(n\omega)|^2\,\mathrm{d}\omega\right] \tag{13}$$

$A(\omega)$ is the A-weighting correction, n is the scaling factor and the angular frequency ω takes the full scale values. One also assumes that the position of the receiver in the scale model is relevant to that at full scale.

What can be done if $\hat{p}_m(n\omega) \neq \hat{p}_v(\omega)$? First, one can relate all the experimental results to what is called the *compensated spectrum*. This relation is established by the following transformation (index c stands for "compensated")

$$\hat{p}_{mc}^2(n\omega) = \hat{p}_m^2(\omega)h_{mv}(\omega), \tag{14}$$

so that the estimated A-weighted *SPL* level can be found according to the following expression

$$L_A^{(v)} = 10\log_{10}\left[\frac{4\pi^2}{p_0^2}\int_0^\infty |A(\omega)\hat{p}_{mc}(n\omega)|^2\,\mathrm{d}\omega\right]. \tag{15}$$

In these expressions the *resemblance function* h_{mv} is defined as

$$h_{mv}(\omega) = \hat{p}_v^2(\omega)/\hat{p}_m^2(n\omega). \tag{16}$$

A similar expression can be derived if the sound pressure in the scale model p_{mi} is measured in N, $1/m$ octave bands (m is an arbitrary integer). In this case the A-weighted broad band sound pressure level in the scale model is calculated as

$$L_A^{(v)} = 10 \log_{10} \left[\sum_{i=1}^{N} A_i^2 p_{mi}^2 h_i / p_0^2 \right], \tag{17}$$

where the *resemblance coefficients* are found as

$$h_i = p_{vi}^2 / p_{mi}^2. \tag{18}$$

Here p_{vi} is the sound pressure measured in $1/m$ octaves at the full scale.

The resemblance function is easily evaluated from a test in which the spectrum of the model source is measured in the general vicinity of the ground, i.e., in the absence of ground reflection. Any obstacles should be removed before the test is carried out, so that

$$h_{mv} = (\hat{p}_v^2(\omega, r_v) / \hat{p}_m^2(n\omega, r_m)) \Delta. \tag{19}$$

Here $\Delta = (r_v/(nr_m))^2$ and r_v and r_m are the distances between the source and the receiver measured at full scale situation and in the model, respectively.

Once the resemblance function is found, the A-weighted sound pressure level can be calculated by expression (17) at any arbitrary point $\bar{r}$ using the actual pressure spectrum obtained in the model experiment. This statement is supported by the superposition principle from which the spectrum of the total acoustic field $\hat{p}_t^2$ in a complex full scale environment can be evaluated as a combination of M multiple reflections and diffraction components $g_j^{(v)}$, i.e.,

$$\hat{p}_t^2(\omega, \bar{r}) = \hat{p}_{ref}^2(\omega, \bar{r}_{ref}) \sum_{j=1}^{M} g_j^{(v)}(\omega, \bar{r}_{ref}, \bar{r}). \tag{20}$$

But, as has already been proved, every individual component of the total acoustic field at full scale can be related to that measured in the scale model as (one refers to 1 m at the full scale and to 0·05 m in the model for $n = 20$)

$$g_j^{(v)}(\omega) = g_j^{(m)}(n\omega) h_{mv}(\omega). \tag{21}$$

Thus the total field at full scale is accurately predicted by the following equation

$$\hat{p}_t^2(\omega, \bar{r}) = \hat{p}_{ref}^2(n\omega, \bar{r}_{ref}) h_{mv}(\omega) \sum_{j=1}^{M} g_j^{(m)}(n\omega, \bar{r}_{ref}^{(m)}, \bar{r}^{(m)}), \tag{22}$$

where the sum $\sum g_j^{(m)}$ is found from the scale model experiment.

APPENDIX B: NOTATION

c	adiabatic speed of sound
EA	excess attenuation
h_{mv}	resemblance function
k	wavenumber in fluid
IL	insertion loss
n	scaling factor

N_{pr}	Prandtl number
p_{ref}	reference pressure
$\hat{p}_v(\omega)$	spectrum emitted by the real vehicle
$\hat{p}_m(\omega)$	spectrum emitted by the model source
R_e	effective flow resistivity
SPL	sound pressure level
V	plane wave reflection coefficient
α	air absorption
β_s	normalised surface admittance
γ	ratio of specific heats
μ	dynamic viscosity
ω	angular frequency